The Vitamin E Radical Probed by Anion Photoelectron Imaging

*Cate S. Anstöter, Christopher W. West, James, N. Bull, and Jan R. R. Verlet**

Department of Chemistry, Durham University, Durham DH1 3LE, United Kingdom

Abstract

The biological antioxidant activity of vitamin E has been related to the stability of the tocopheroxyl radical. Using anion photoelectron imaging and electronic structure calculations, the four tocopheroxyl components of vitamin E have been studied in the gas-phase and have yielded the adiabatic detachment energies of the α-, β/γ- and δ-tocopheroxyl radicals. Using these values, the bond dissociation enthalpy of the O-H bond of tocopherol has been estimated and is consistent with previous studies and with the trends in biological activity. Differences in the photoelectron angular distributions have been interpreted to result from changes in the symmetry of the molecular orbitals from which the electron was detached.

*j.r.r.verlet@durham.ac.uk

Introduction

Antioxidants are molecules that can inhibit or reverse oxidative damage and are essential to the maintenance of biological systems by minimizing oxidative stress.[1] The lipophilic vitamin E class of molecules is the major lipid soluble, peroxyl-radical trapping, chain breaking antioxidant in blood plasma,[2–4] and in normal and cancerous tissues.[5] There are four variants that constitute naturally occurring vitamin E, denoted α-, β-, γ-, and δ-tocopherol. The most important biological function of vitamin E is as a peroxyl radical scavenger[6] in which a hydrogen atom is transferred from the phenol group to generate the resonance stabilised tocopheroxyl radical, $Toc^{\bullet}$. The structures of the four tocopheroxyl radicals are shown in Figure 1, where δ-$Toc^{\bullet}$ is the simplest structural unit with only the R_1 position methylated. The β- and γ- $Toc^{\bullet}$ have a second methyl group in one of the two available ortho-sites relative to the phenolic oxygen (R_2 or R_3), while the ring is fully methylated for α-$Toc^{\bullet}$.

The antioxidant action of the tocopherols has been attributed to interruption of the propagation of lipid peroxyl radicals ($LOO^{\bullet}$), by instead forming $Toc^{\bullet}$, thereby inhibiting the peroxidation process that would otherwise result in membrane damage to cells.[7] Once formed, $Toc^{\bullet}$ is relatively unreactive and does not propagate in the same way as the lipid peroxyl free radical.[8] The mechanism has been extensively studied and can be expressed as,[8–11]

$$LOO^{\bullet} + TocH \xrightarrow{k_{inh}} LOOH + Toc^{\bullet}, \quad (1)$$

where TocH is the tocopherol with the phenolic hydrogen present. This reaction proceeds much faster than propagation reactions with unperoxidised lipids, due to a higher propensity of hydrogen donation in TocH, which can be attributed to a reduced bond dissociation

enthalpy (BDE). Of the vitamin E group, α-TocH has the largest second order rate constant[12] and is the only tocopherol that meets human vitamin E requirements.[6] The β- and γ-TocH are only slightly less reactive and have no significant differences in reactivity to one another. Finally, δ-TocH is the least reactive member, reflected in a reduced rate constant.[8] TocH molecules primarily protect unsaturated fatty acids against oxidative damage and neoplastic transformation, arising from oxygen-derived radicals and nitrogen oxides, respectively. The α-TocH exhibits an enhanced bioactivity with respect to the oxygen radicals, whereas γ-TocH shows superior and unique reactivity towards NO_2.[13] Furthermore, it has been proposed that γ-TocH has an additional specific chemical role, disparate to radical scavenging; it can trap electrophilic mutagens in lipophilic compartments due to its nucleophilic properties.[14] A common electrophilic mutagen is peroxynitrite and, through scavenging this mutagen, γ-TocH can protect proteins, lipids and DNA from peroxynitrite-dependent stress.

A comprehensive survey[15] of the effect of ring substituents on chain breaking phenolic antioxidants determined that the reaction is enhanced by a 4-methoxy group and methyl groups in the remaining 2-, 3-, 5-, and 6- positions. The phenoxyl oxygen is drastically hindered from participating in further chain transfer reactions through both steric shielding by methyl groups in both 2- and 3-positions and by the electron-donating methoxy group in the 4-position. The reactive moiety of the TocH is the phenolic fragment of the molecule, yet TocH is much more reactive toward peroxy radicals than other structurally related compounds. This difference is attributed to a steric imposition on rotational motion, which maximizes the overlap between the lone pair of the methoxy group with the radical in $Toc^{\bullet}$, experimentally confirmed by electron spin resonance.[8] The interaction of the oxygen lone pair with the radical increases the inherent stability of $Toc^{\bullet}$ and the rate of hydrogen transfer from TocH. [2]

Despite the wealth of information gained over many decades about the reactivity and stability of TocH and Toc$^{\bullet}$, fundamental properties such as the electron affinity of Toc$^{\bullet}$, and its electronic structure are poorly quantified. Characterisation of these properties can provide insight into the dissociation energy of the Toc-H bond. These physical properties pertain directly to the antioxidant nature of vitamin E. In the present work, we have studied the electronic structure of the Toc$^{\bullet}$ using anion photoelectron (PE) imaging and quantum calculations. Specifically, PE spectroscopy of the deprotonated anion of the parent TocH molecule provides the electron affinity of Toc$^{\bullet}$ as well as information about its excited states and, when combined with quantum calculations, can provide insight into the electronic structure of Toc$^{\bullet}$. The latter is particularly insightful when considering its reactivity as a chain-breaking antioxidant.

Experimental

The experimental setup and methodology has been previously described in detail,[16,17] and only details relevant to the current experiment are provided. A sample of mixed α-, β-, γ- and δ-TocH (Sigma Aldrich, Food grade, Kosher) was used without further purification. Isolated deprotonated anions of TocH, Toc^{-}, were produced by electrospray ionisation of a ~1 mM solution in MeOH. The ionisation source was coupled to vacuum by a transfer capillary and the anions were subsequently trapped in a home-built radio frequency ring-electrode ion trap. The ion packet was pulsed out of the trap at a rate of 10 Hz. Ion packets were mass separated using time-of-flight and at the focus of the mass-spectrometer, the mass-selected ion packet was irradiated. The interaction region is situated at the centre of a velocity-map-imaging[18] PE spectrometer.[19] The mass spectrum showed well-separated peaks from δ-Toc^{-} (*m/z* = 401.7) and α-Toc^{-} (*m/z* = 429.7). As β- and γ-Toc^{-} (*m/z* = 415.7) are mass-degenerate, the PE spectra of this mass-selected ion packet contain both species. The isolated *x*-Toc^{-}

(where *x* is α, β/γ, or δ) ion packet was irradiated by nanosecond laser pulses at 3.88 eV (320 nm), generated by an optical parametric oscillator (Horizon I, Continuum) pumped by an Nd:YAG laser (Surelite-II, Continuum). The photoelectron velocity-mapped images were measured using a dual multichannel-plate detector coupled to a phosphor screen, which was monitored using a CCD camera. Raw PE images were deconvoluted using the polar-onion peeling algorithm[20] in order to extract the PE spectra and PE angular distributions. PE spectra were calibrated from the atomic I^- spectrum and have a resolution of ~5%.

Computational Details

Density functional theory (DFT) calculations were performed using the Gaussian 09 computational package.[21] DFT calculations used both the CAM-B3LYP[22] and ωB97XD[23] functionals with the aug-cc-pVDZ basis set, chosen because of their performance in calculations of anionic species.[24–27] Both functionals gave good agreement in preliminary calculations; here we present the CAM-B3LYP results. The equilibrium geometries of the dehydrogenated neutral radical $Toc^{\bullet}$ and the negatively charged deprotonated Toc^- were optimized at this level of theory and confirmed to represent the geometrical minimum through vibrational frequency analysis. Vibrational frequency calculations allowed for the simulation of the experimentally measured PE spectra. Time-dependent density functional theory (TD-DFT) calculations provided approximate excited state energetics of $Toc^{\bullet}$.

The primary role of the phytyl moiety ($C_{16}H_{33}$) is to increase the solubility of $Toc^{\bullet}$ in lipid membranes and, as such, has only a minor role in the antioxidant activity of $Toc^{\bullet}$.[11] Although all experimental work refers to the full $Toc^{\bullet}$ structures, the phytyl chain dramatically increases the computational cost, so was reduced to a methyl group in all calculations herein. For the α-TocH this reduction in chain length makes the molecule chemically equivalent to 2,2,5,7,8-pentamethyl-6-hydrochromane, which has been shown to

have a similar reactivity profile to α-Toc,[8] indicating that that the antioxidant reactivity of the molecules is predominantly determined by the chromane moiety. Hence, the removal of the phytyl chain for computational tractability is expected to yield results directly comparable with the full tocopherols.

Results

PE spectra recorded at 3.88 eV (320 nm) for α-Toc$^-$, β/γ-Toc$^-$, and δ-Toc$^-$ are shown in Figure 2. The PE spectra for the three *x*-Toc$^-$ are broadly similar. They all have a PE feature with an electron binding energy (eBE) peaking around 2.2 eV. The PE spectrum for β/γ-Toc$^-$ has an additional feature at higher binding energy, peaking around eBE ~ 3.4 eV. The experimental vertical detachment energy (VDE) corresponds to the peak position of the lowest eBE feature. The adiabatic detachment energy (ADE) has been estimated by extrapolating the lowest eBE edge.[28] These values for the different *x*-Toc$^-$ species are summarised in Table 1 and show that both the VDE and ADE increase with decreasing methyl substitutions on the phenoxyl ring.

In addition to the spectral information, PE imaging provides PE angular distributions associated with the photodetachment. In the imaging reconstruction, PE angular distributions, $I(\theta)$, are quantified using the conventional β_2 parameter[29]

$$I(\theta) \propto 1 + \tfrac{1}{2}\beta_2(3\cos^2\theta - 1) \quad (2)$$

where θ is the angle between the polarisation vector of the light and the PE ejection direction. The β_2 parameters averaged over the direct photodetachment band for each of *x*-Toc$^-$ are given in Table 1. For α-Toc$^-$ and β/γ-Toc$^-$, $\beta_2 \sim 0$, which corresponds to an isotropic electron ejection. For δ-Toc$^-$, β_2 is negative, corresponding to an electron ejection that is

predominantly perpendicular to the laser polarisation axis. The β_2 parameters for each of *x*-Toc$^-$ are constant over the direct photodetachment band.

Results of DFT calculations on *x*-Toc$^-$ are summarised in Table 1. Vibrational frequency calculations allowed the simulation of the photodetachment spectra for all four of the *x*-Toc$^-$ and provided guidance as to whether or not the β-Toc$^-$ and γ-Toc$^-$ that are indistinguishable by mass could be distinguished in the PE spectra. The simulated PE spectra are included in Figure 2 and show that, although there are slight differences in the calculated ADE (see Table 1), these are well within the spectral width of the experimental PE peaks. The similarities in the calculated PE spectra of β-Toc$^-$ and γ-Toc$^-$, which also look very similar to those of α-Toc$^-$ and δ-Toc$^-$, demonstrate the minor effect of position of a methyl groups on the ADE. While a single dominant PE feature was observed for α-Toc$^-$ and δ-Toc$^-$, an additional peak at higher binding energies was seen in the PE spectrum of β/γ-Toc$^-$. An accompanying change in the β_2 parameter (–0.24 ± 0.14) was observed across this PE peak. TD-DFT calculations identified doublet excited states of neutral *x*-Toc$^\bullet$ all at ~1.5 eV above the neutral ground state.

Discussion

Both the PE spectra and DFT calculations show that there is a small increase in VDE and ADE with the decreasing number of methyl groups on the phenoxyl ring. The main reason for these small changes can be inferred from the molecular orbitals (MOs) from which the electron is removed. In Figure 3, the highest occupied MO (HOMO) is shown for the four *x*-Toc$^-$ derivatives. The direct detachment feature at highest binding energy corresponds to the loss of an electron from the doubly-occupied HOMO in the anion – see Figure 4. The density of the HOMO is localised primarily on the phenoxyl ring with a small contribution on the methoxy group in the nonaromatic ring. The HOMO has the appearance of a quinoidal

MO because of the chromane moiety and the stability of the radical arises from the resonance stabilisation of the quinone structure.[30] The modest increase in VDE and ADE is attributed to the small electron density of the HOMO on the methyl groups.

Additional experimental evidence that some of the HOMO density resides on the methyl groups can be tentatively gained from the PE angular distributions. Although none of the *x*-Toc$^-$ molecular geometries contain a symmetry axis and would typically lead to isotropic PE angular distributions, the HOMO of *x*-Toc$^-$ is surprisingly symmetric. The small contribution on the methyl groups of β/γ-Toc$^-$ breaks this symmetry, while the HOMO of α-Toc$^-$ and δ-Toc$^-$ retains the symmetry. One might therefore expect that, if any anisotropy in the PE angular distribution were to be observed, it would be most prominent in α-Toc$^-$ and δ-Toc$^-$. However, the calculations were performed at 0 K, which assumes the methyl groups are rigid. At finite temperature, rotational freedom is likely to average out any PE anisotropy for [α-Toc]$^-$ leading to an isotropic PE angular distribution. For [δ-Toc]$^-$, which has only the meta-methyl group on the phenoxyl-ring, the HOMO is solely localised on the quinoidal ring such that the symmetry is retained which is reflected in the PE angular distribution as an observable anisotropy. While it can be difficult to confidently account for anisotropy differences, the experimental results clearly show a significant difference between δ-Toc$^-$ and the other *x*-Toc$^-$ species. A common cause discussed in the literature is that changes in anisotropy can result from differences in photodetachment cross-sections.[29] However, in the present case, the PE spectra of δ-Toc$^-$ and α-Toc$^-$ (and general electronic structure) are essentially identical, which suggests more subtle differences in electron density rather than differences in photodetachment cross-sections.

Based on the MOs in Figure 3, removal of an electron from the HOMO will lead to structural changes involving primarily contraction of the C–O bonds and bond alterations in the ring. However, these changes are rather small as suggested by the simulated

photodetachment spectra that are dominated by the 0-0 transition. The experimental spectral width in Figure 2 is therefore likely to be related to the finite temperature (~300 K) of the ions in the experiment. Although the chromane ring is probably planar and rigid, as evidenced by the observed anisotropy of the PE angular distribution of δ-Toc$^-$, the long phytyl chain that extends from the molecule is flexible and may interact with the HOMO, leading to the observed spectral widths. We have recently observed similar interactions in the PE spectra of a deprotonated carboxylic acid group attached by an aliphatic chain to a phenyl group.[31] The interaction of an aliphatic chain with an aromatic ring has also been observed in experimental and computational studies of the ionization of neutral molecules.[32–34] Perhaps surprising is that the direct photodetachment from δ-Toc$^-$ shows the most significant broadening. This result is reconciled by considering the steric influence of the methyl groups. For δ-Toc$^-$, there is no steric hindrance for the phytyl chain to interact with the HOMO, while all the others, and in particular α-Toc$^-$, have methyl groups that do not have a high HOMO density that could restrict the interaction of the phytyl chain with the HOMO. Hence, the interaction of the phytyl chain with the HOMO may be expected to be largest for δ-Toc$^-$. In a biological system, the hydrophobic phytyl chain is deemed not to interact with the antioxidant behaviour of vitamin E as its main role is to increase solubility in lipid membranes and so, unlike the gas-phase, the chain is likely to be well-solvated in the lipid membrane and non-interacting with the head-group.

The observed trends of the VDE and ADE are consistent with chemical and physical properties of *x*-Toc$^-$. Electron donor groups, such as methyl, tend to destabilize the O-H bond in phenol and enhance the stability of the corresponding phenoxyl radical.[35] This effect is demonstrated when comparing the measured rates of reactivity of the tocopherols, where the most bioactive component of vitamin E is α-TocH and the least active is the smallest δ-TocH. An increase in number of substituted methyl groups causes an increased efficiency of

the relative H-atom donating abilities of the different tocopherols. This trend is approximately constant whether the rates were measured in organic solvents or detergent supported lipids.[6] The relative efficiencies of *x*-TocH *in vitro* appear similar,[8] while *in vivo* the increased antioxidant potency of α-TocH is due to preferential absorption by the liver.[6]

A number of previous studies have presented estimates for the OH bond dissociation enthalpy (BDE) of the tocopherol family of molecules,[36–41] which is directly linked to their antioxidant activity. Phenol has a higher BDE than any of the tocopherols, differing by +0.42 eV compared to the most active α-TocH,[37] and a reduced BDE of the OH has been used as the primary criterion in the search for more active antioxidants than the naturally abundant α-TocH.[42,43] Our experiments have determined the ADE of *x*-Toc$^-$, which is equivalent to the adiabatic electron affinity of *x*-Toc$^\bullet$, and can be used to provide a determination of the OH BDE by invoking a thermodynamic cycle proposed by Blanksby and Ellison.[44] For a general R-H bond,

$$\mathrm{BDE(R\text{-}H)} = \Delta_{\mathrm{acid}}H\mathrm{(R\text{-}H)} + \mathrm{ADE(R)} - \mathrm{IP(H)}, \qquad (3)$$

where $\Delta_{\mathrm{acid}}H$(R-H) is the enthalpy change for the reaction $\mathrm{RH} \rightarrow \mathrm{R}^- + \mathrm{H}^+$, ADE(R) is the electron affinity of R, and IP(H) = 13.6 eV is the ionisation energy of the H atom. To the best of our knowledge, the value for $\Delta_{\mathrm{acid}}H$ of any *x*-TocH has not been determined and, as such, it was not possible to determine the correct values using the above thermodynamic cycle. Instead, we use the $\Delta_{\mathrm{acid}}H$ value of phenol (15.11 eV),[37] which has been well-documented and should be close to that for *x*-TocH. The calculated BDE are included in Table 1 and show that α-TocH has the lowest value, consistent with its highest antioxidant activity. The remaining tocopherols mimic the antioxidant reactivity trend described earlier, with the least biologically active δ-TocH having the highest BDE. We note that the cycle can also be used

to verify the ADE of the phenoxy radical, which should be +0.42 eV relative to α-TocH.[37] This yields an ADE = 2.13 eV for the phenoxy radical, which compares very well with the measured value of 2.25 eV by Lineberger and coworkers.[45] Although an experimental determination of $\Delta_{acid}H$ is desirable, this is beyond the scope of the present study.

Finally, we comment on the peak at higher eBE seen in the PE spectrum of β/γ-Toc$^-$. Our calculations show the first excited state for all *x*-Toc$^\bullet$ corresponds to excitation of HOMO – 2 to the singly occupied HOMO, as shown in Figure 4, and is situated about 1.5 eV above the doublet ground state. This state can be compared to the first excited state of the phenoxy-radical, measured at 1.06 eV using anion PE spectroscopy,[45] which reveals that the energy gap is larger in *x*-Toc$^\bullet$ than the phenoxy radical. This is consistent with the fact that the the *x*-Toc$^\bullet$ radical has a quinoidal electronic structure. Experimentally, it is surprising that there is such an observable difference in excited states of β/γ-Toc$^\bullet$, compared to α-Toc$^\bullet$ and δ-Toc$^\bullet$. However, we note that there also an increase in PE signal at high eBE for α-Toc$^\bullet$ and δ-Toc$^\bullet$ suggestive of a nearby excited state of the neutral, and the PE signal of these may be reduced because of threshold effects.[46] Alternatively, the differences in appearance of the PE spectra could be due resonances in the continuum.[47–49] However, this seems unlikely given that the electronic structures of *x*-Toc$^\bullet$ are similar and the fact that the features are well-separated. Nevertheless, performing these experiments at a range of photon energies could probe this possibility further.

Conclusions

In summary, we have presented photoelectron spectra complemented with electronic structure calculations of the four tocopheroxyl radicals responsible for the antioxidant action of naturally occurring vitamin E. The adiabatic detachment energies (equivalent to electron affinities) of α-, β-/γ-, and δ-Toc$^\bullet$ have been determined and from these values the bond

dissociation energies have been estimated and found to be in good agreement with previous measured values. The trends noted in terms of physical and chemical properties and biological activity across the series are consistent with the photoelectron spectroscopy.

Acknowledgement

We are grateful to Andrew Beeby for helpful discussions and Joshua Rogers for preliminary calculations. This work was funded by the ERC (Starting Grant 306536) and the EPSRC.

References

(1) Gutteridge, J. M. C.; Halliwell, B. Antioxidants: Molecules, Medicines, and Myths. *Biochem. Biophys. Res. Commun.* **2010**, *393* (4), 561–564.

(2) Burton, G. W.; Ingold, K. U. Vitamin E: Application of the Principles of Physical Organic Chemistry to the Exploration of Its Structure and Function. *Acc. Chem. Res.* **1986**, *19* (7), 194–201.

(3) Bowry, V. W.; Ingold, K. U. The Unexpected Role of Vitamin E (α-Tocopherol) in the Peroxidation of Human Low-Density Lipoprotein. *Acc. Chem. Res.* **1999**, *32* (1), 27–34.

(4) Ingold, K. U.; Webb, A. C.; Witter, D.; Burton, G. W.; Metcalfe, T. A.; Muller, D. P. R. Vitamin E Remains the Major Lipid-Soluble, Chain-Breaking Antioxidant in Human Plasma Even in Individuals Suffering Severe Vitamin E Deficiency. *Arch. Biochem. Biophys.* **1987**, *259* (1), 224–225.

(5) Slater, T. F.; Cheeseman, K. H.; Benedetto, C.; Collins, M.; Burtont, G. W.; Ingold, K. U. Studies on the Hyperplasia (’regeneration') of the Rat Liver Following Partial

Hepatectomy. *Biochem. J.* **1990**, *265*, 51–59.

(6) Traber, M. G.; Atkinson, J. Vitamin E, Antioxidant and Nothing More. *Free Radic. Biol. Med.* **2007**, *43* (1), 4–15.

(7) Parthasarathy, S.; Steinberg, D.; Witztum, J. L. The Role of Oxidised Low-Density Lipoproteins in the Pathogenesis of Atherosclerosis. *Annu. Rev. Med.* **1992**, *43*, 219–225.

(8) Burton, G. W.; Ingold, K. U. Autoxidation of Biological Molecules. 1. Antioxidant Activity of Vitamin E and Related Chain-Breaking Phenolic Antioxidants in Vitro. *J. Am. Chem. Soc.* **1981**, *103* (24), 6472–6477.

(9) Girotti, A. W. Mechanisms of Lipid Peroxidation. *J. Free Radic. Biol. Med.* **1985**, *1*, 87–95.

(10) Niki, E. Antioxidants in Relation to Lipid Peroxidation. *Chem. Phys. Lipids* **1987**, *44*, 227–253.

(11) Kamal-Eldin, A.; Appelqvist, L.-Å. The Chemistry and Antioxidant Properties of Tocopherols and Tocotrienols. *Lipids* **1996**, *31* (7), 671–701.

(12) Mukai, K.; Tokunaga, A.; Itoh, S.; Kanesaki, Y.; Ohara, K.; Nagaoka, S.-I.; Abe, K. Structure-Activity Relationship of the Free-Radical-Scavenging Reaction by Vitamin E (Alpha-, Beta-, Gamma-, Delta-Tocopherols) and Ubiquinol-10: pH Dependence of the Reaction Rates. *J. Phys. Chem. B* **2007**, *111* (3), 652–662.

(13) Cooney, R. Products of γ-Tocopherol Reaction with NO_2 and Their Formation in Rat Insulinoma (RINm5F) Cells. *Free Radic. Biol. Med.* **1995**, *19* (3), 259–269.

(14) Brigelius-Flohé, R.; Traber, M. G. Vitamin E: Function and Metabolism. *FASEB J.* **1999**, *13* (10), 1145–1155.

(15) Howard, J. A.; Ingold, K. U. The Inhibited Autoxidation of Styrene Part III. The Relative Inhibiting Efficiencies of Ortho-Alkyl Phenols. *Can. J. Chem.* **1963**, *41*,

2800–2806.

(16) Horke, D. A.; Verlet, J. R. R. Time-Resolved Photoelectron Imaging of the Chloranil Radical Anion: Ultrafast Relaxation of Electronically Excited Electron Acceptor States. *Phys. Chem. Chem. Phys.* **2011**, *13* (43), 19546–19552.

(17) Lecointre, J.; Roberts, G. M.; Horke, D. A.; Verlet, J. R. R. Ultrafast Relaxation Dynamics Observed through Time-Resolved Photoelectron Angular Distributions. *J. Phys. Chem. A* **2010**, *114* (42), 11216–11224.

(18) Eppink, A. T. J. B.; Parker, D. H. Velocity Map Imaging of Ions and Electrons Using Electrostatic Lenses: Application in Photoelectron and Photofragment Ion Imaging of Molecular Oxygen. *Rev. Sci. Instrum.* **1997**, *68* (9), 3477–3484.

(19) Horke, D. A.; Roberts, G. M.; Lecointre, J.; Verlet, J. R. R. Velocity-Map Imaging at Low Extraction Fields. *Rev. Sci. Instrum.* **2012**, *83* (6), 063101.

(20) Roberts, G. M.; Nixon, J. L.; Lecointre, J.; Wrede, E.; Verlet, J. R. R. Toward Real-Time Charged-Particle Image Reconstruction Using Polar Onion-Peeling. *Rev. Sci. Instrum.* **2009**, *80* (5), 053104.

(21) Frisch, M. J.; Trucks, G. W.; Schlegel, H. B.; Scuseria, G. E.; Robb, M. A.; Cheeseman, J. R.; Scalmani, G.; Barone, V.; Mennucci, B.; Petersson, G. A.; et al. Gaussian 09 Revision E.01. Gaussian, Inc.: Wallingford CT 2009.

(22) Yanai, T.; Tew, D. P.; Handy, N. C. A New Hybrid Exchange–correlation Functional Using the Coulomb-Attenuating Method (CAM-B3LYP). *Chem. Phys. Lett.* **2004**, *393* (1-3), 51–57.

(23) Chai, J.-D.; Head-Gordon, M. Long-Range Corrected Hybrid Density Functionals with Damped Atom–atom Dispersion Corrections. *Phys. Chem. Chem. Phys.* **2008**, *10* (44), 6615.

(24) Peach, M. J. G.; Tellgren, E. I.; Sałek, P.; Helgaker, T.; Tozer, D. J. Structural and

Electronic Properties of Polyacetylene and Polyyne from Hybrid and Coulomb-Attenuated Density Functionals. *J. Phys. Chem. A* **2007**, *111* (46), 11930–11935.

(25) Cai, Z.-L.; Crossley, M. J.; Reimers, J. R.; Kobayashi, R.; Amos, R. D. Density Functional Theory for Charge Transfer: The Nature of the N-Bands of Porphyrins and Chlorophylls Revealed through CAM-B3LYP, CASPT2, and SAC-CI Calculations. *J. Phys. Chem. B* **2006**, *110* (31), 15624–15632.

(26) Cohen, A. J.; Mori-Sanchez, P.; Yang, W. Insights into Current Limitations of Density Functional Theory. *Science* **2008**, *321* (5890), 792–794.

(27) Sherrill, C. D. Frontiers in Electronic Structure Theory. *J. Chem. Phys.* **2010**, *132* (11), 110902.

(28) Horke, D. A.; Verlet, J. R. R. Photoelectron Spectroscopy of the Model GFP Chromophore Anion. *Phys. Chem. Chem. Phys.* **2012**, *14* (24), 8511–8515.

(29) Cooper, J.; Zare, R. N. Angular Distribution of Photoelectrons. *J. Chem. Phys.* **1968**, *48* (2), 942–943.

(30) Eitenmiller, R. R.; Lee, J. *Vitamin E: Food Chemistry, Composition, and Analysis Food Science and Technology*; Marcel Dekker: New York, 2004.

(31) Anstöter, C. S.; West, C. W.; Bull, J. N.; Verlet, J. R. R. Unpublished Results.

(32) Tong, X.; Ford, M. S.; Dessent, C. E. H.; Müller-Dethlefs, K. The Effect of Conformation on the Ionization Energetics of N-Butylbenzene. I. A Threshold Ionization Study. *J. Chem. Phys.* **2003**, *119* (24), 12908.

(33) Ford, M. S.; Tong, X.; Dessent, C. E. H.; Müller-Dethlefs, K. The Effect of Conformation on the Ionization Energetics of N-Butylbenzene. II. A Zero Electron Kinetic Energy Photoelectron Spectroscopy Study with Partial Rotational Resolution. *J. Chem. Phys.* **2003**, *119* (24), 12914.

(34) Halbert, S.; Clavaguéra, C.; Bouchoux, G. The Shape of Gaseous N-Butylbenzene:

Assessment of Computational Methods and Comparison with Experiments. *J. Comput. Chem.* **2011**, *32* (8), 1550–1560.

(35) Rappoport, Z. *The Chemistry of Phenols*; Rappoport, Z., Ed.; The Chemistry of Functional Groups; John Wiley & Sons, Ltd: Chichester, UK, 2003.

(36) Wayner, D. D. M.; Lusztyk, E.; Ingold, K. U.; Mulder, P. Application of Photoacoustic Calorimetry to the Measurement of the O−H Bond Strength in Vitamin E (α- and δ-Tocopherol) and Related Phenolic Antioxidants. *J. Org. Chem.* **1996**, *61* (18), 6430–6433.

(37) Borges dos Santos, R. M.; Martinho Simões, J. A. Energetics of the O–H Bond in Phenol and Substituted Phenols: A Critical Evaluation of Literature Data. *J. Phys. Chem. Ref. Data* **1998**, *27* (3), 707–739.

(38) Tafazoli, S.; Wright, J. S.; O'Brien, P. J. Prooxidant and Antioxidant Activity of Vitamin E Analogues and Troglitazone. *Chem. Res. Toxicol.* **2005**, *18* (10), 1567–1574.

(39) Shanks, D.; Amorati, R.; Fumo, M. G.; Pedulli, G. F.; Valgimigli, L.; Engman, L. Synthesis and Antioxidant Profile of All-Rac-α-Selenotocopherol. *J. Org. Chem.* **2006**, *71* (3), 1033–1038.

(40) Nix, M. G. D.; Devine, A. L.; Cronin, B.; Dixon, R. N.; Ashfold, M. N. R. High Resolution Photofragment Translational Spectroscopy Studies of the near Ultraviolet Photolysis of Phenol. *J. Chem. Phys.* **2006**, *125* (13), 133318.

(41) Dorofeeva, O. V.; Ryzhova, O. N. Enthalpy of Formation and O–H Bond Dissociation Enthalpy of Phenol: Inconsistency between Theory and Experiment. *J. Phys. Chem. A* **2016**, *120* (15), 2471–2479.

(42) Hussain, H. H.; Babic, G.; Durst, T.; Wright, J. S.; Flueraru, M.; Chichirau, A.; Chepelev, L. L. Development of Novel Antioxidants: Design, Synthesis, and

Reactivity. *J. Org. Chem.* **2003**, *68* (18), 7023–7032.

(43) Valgimigli, L.; Pratt, D. A. Maximizing the Reactivity of Phenolic and Aminic Radical-Trapping Antioxidants: Just Add Nitrogen! *Acc. Chem. Res.* **2015**, *48* (4), 966–975.

(44) Blanksby, S. J.; Ellison, G. B. Bond Dissociation Energies of Organic Molecules. *Acc. Chem. Res.* **2003**, *36* (4), 255–263.

(45) Gunion, R. F.; Gilles, M. K.; Polak, M. L.; Lineberger, W. C. Ultraviolet Photoelectron Spectroscopy of the Phenide, Benzyl and Phenoxide Anions, with Ab Initio Calculations. *Int. J. Mass Spectrom. Ion Process.* **1992**, *117*, 601–620.

(46) Wigner, E. P. On the Behavior of Cross Sections Near Thresholds. *Phys. Rev.* **1948**, *73* (9), 1002–1009.

(47) West, C. W.; Bull, J. N.; Hudson, A. S.; Cobb, S. L.; Verlet, J. R. R. Excited State Dynamics of the Isolated Green Fluorescent Protein Chromophore Anion Following UV Excitation. *J. Phys. Chem. B* **2015**, *119* (10), 3982–3987.

(48) West, C. W.; Bull, J. N.; Antonkov, E.; Verlet, J. R. R. Anion Resonances of Para-Benzoquinone Probed by Frequency-Resolved Photoelectron Imaging. *J. Phys. Chem. A* **2014**, *118*, 11346–11354.

(49) Horke, D. A.; Li, Q.; Blancafort, L.; Verlet, J. R. R. Ultrafast Above-Threshold Dynamics of the Radical Anion of a Prototypical Quinone Electron-Acceptor. *Nat. Chem.* **2013**, *5* (8), 711–717.

x-Toc$^-$	VDE_{exp}	ADE_{exp}	ADE_{calc}	β_2	BDE(O-H)
α	2.14 ± 0.10	1.71 ± 0.10	1.64	–0.05 ± 0.09	3.25
β/ γ	2.22 ± 0.10	1.78 ± 0.10	1.68/1.70	–0.02 ± 0.12	3.32
δ	2.32 ± 0.10	1.81 ± 0.10	1.75	–0.31 ± 0.10	3.35

Table 1. Experimentally determined vertical detachment energies (VDE_{exp}); adiabatic detachment energies determined from experiment (ADE_{exp}) and from zero-point corrected calculations (ADE_{calc}); β_2 anisotropy parameters; and bond dissociation energies (BDE) of the O-H bond in *x*-TocH determined from the ADE_{exp} values. All energies are given in units of eV.

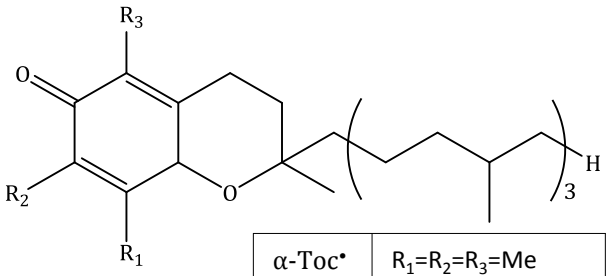

α-Toc•	$R_1=R_2=R_3=Me$
β-Toc•	$R_1=R_3=Me$; $R_2=H$
γ-Toc•	$R_1=R_2=Me$; $R_3=H$
δ-Toc•	$R_1=Me$; $R_2=R_3=H$

Figure 1: Molecular structures of deprotonated vitamin E (α-, β-, γ-, and δ-tocopheroxyl radical).

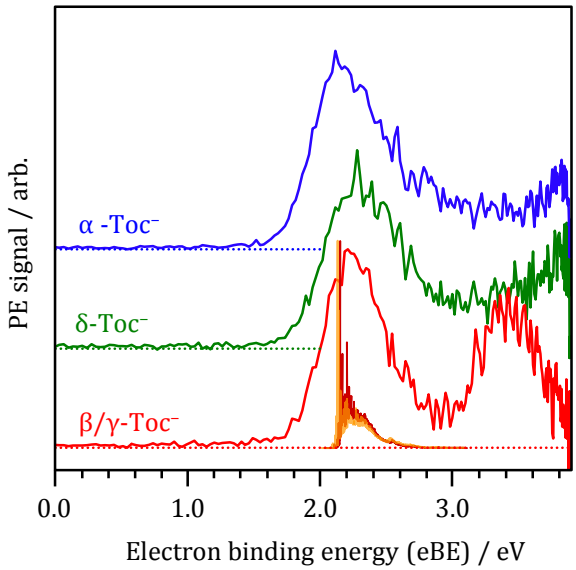

Figure 2. Photoelectron spectra taken at *hv* = 3.88 eV for α- (blue), β-/γ- (red) and δ-Toc– (green). Also included are calculated photodetachment spectra for the two isobaric species, β- and γ -Toc⁻, given in orange and red respectively.

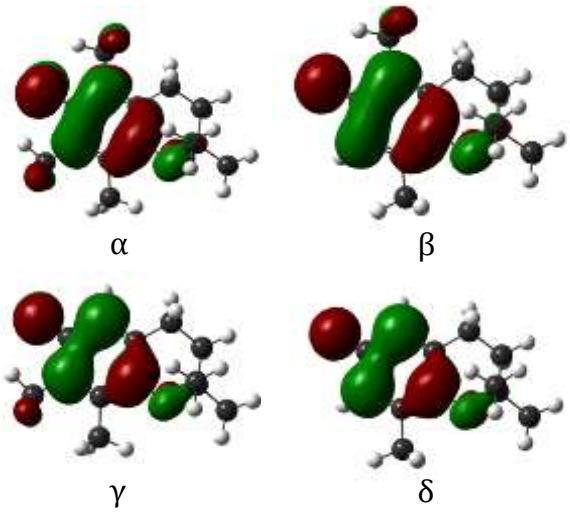

Figure 3: Calculated highest occupied molecular orbitals for the four *x*-Toc^{-} anions at CAM-B3LYP/aug-cc-pVDZ level of theory.

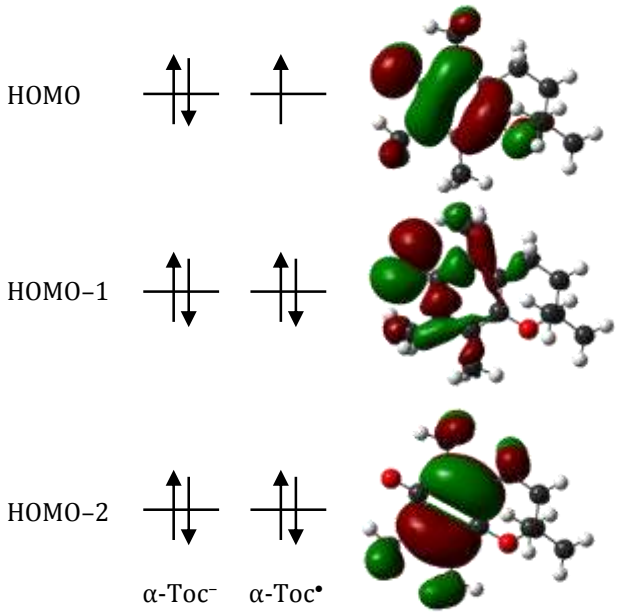

Figure 4: Calculated frontier orbitals of α-Toc$^-$ at CAM-B3LYP/aug-cc-pVDZ level of theory. The occupancy of the anion and radical are shown. The frontier orbitals have minimal variation between the *x*-Toc molecules, differing only on density on the substituted methyl groups.

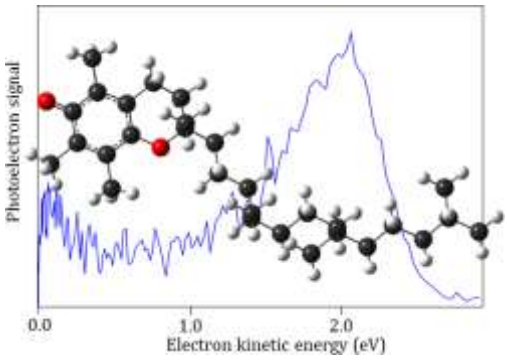

Table of content image